Inclusive Deep Inelastic Scattering at HERA and related phenomenology

Fabian Zomer

IN2P3-CNRS and Université de Paris-Sud, Laboratoire de l'Accélérateur Linéaire, Bâtiment 200, F-91898 BP 34 Orsay Cedex, France

Abstract. Recent measurements of inclusive deep inelastic scattering differential cross-section in the range $1.5\text{GeV}^2 \leq Q^2 \leq 30000\text{GeV}^2$ and $5 \cdot 10^{-6} \leq x \leq 0.65$ are presented. Phenomenological analyses performed from these measurements are also described.

1 Introduction

In the Deep Inelastic Scattering (DIS) processes observed at HERA, a lepton $\ell = e^{\pm}$ of 27.5 GeV interacts with a proton P of 920 GeV yielding a lepton ℓ' and a set of hadrons X in the final state. Following the nature of ℓ' the interaction proceed via a neutral ($\ell' = e^{\pm}$) current (NC) or a charged ($\ell' = \nu_e, \bar{\nu}_e$) current (CC). DIS events are collected in the H1 and ZEUS experiments [1] which are located at the two $e^{\pm}P$ interaction points of HERA.

The kinematics of the DIS inclusive processes, $\ell(k) + P(p) \to \ell'(k') + X$, is determined by two independent kinematic variables, besides the energy of the incoming lepton and proton. One usually chooses them among the four Lorentz invariants

$$Q^2 \equiv -q^2 = -(k - k')^2,\ x = \frac{Q^2}{2p \cdot q}\ ,\ y = \frac{p \cdot q}{p \cdot k},\ W^2 = (q + p)^2,$$

at HERA one can neglect the lepton and proton masses so that the useful relation $Q^2 = xys$ holds. These kinematic variables are obtained experimentally by measuring the momentum and/or the hadronic energy, the direction of the scattered lepton and/or the hadronic energy flow.

In this communication we shall restrict ourselves to the cross-section measurements at HERA in the medium $1.5\ \text{GeV}^2 \leq Q^2 < 150\ \text{GeV}^2$ and high $150\ \text{GeV}^2 \leq Q^2 \leq 30000\ \text{GeV}^2$ domain of the DIS regime. During the past, a large number of precise measurements have been performed in the medium Q^2 region by fixed target experiments [2]. With HERA, three major improvements may be noticed:

- an extension of the Q^2 domain toward high-Q^2 but also downward small-$x \approx 10^{-6}$ regions;
- an almost hermetic (4π) detection of the final state leading to the determination of the energies and angles of the scaterred leptons and of the produced hadrons;

- from the previous items it follows that the detection of both NC and CC is feasible in the same detector and during the same data tacking;

The somehow arbitrary distinction between low and high Q^2 is related to different physics interests. In both region perturbative Quantum-Chromo-Dynamic (pQCD) describes HERA data [3]. In that direction, the pQCD analysis of medium-Q^2 data is a part of a long tradition [4] from which the parton distribution of the nucleon and the strong coupling constant α_s are extracted. On the top of that, very high-$Q^2 \approx M_Z^2$ NC and CC data open a field of research in the electroweak physics up to now reserved, in DIS, to neutrino beam experiments.

The rest of this communication is organized as follows. In section 2 the measurements of CC and NC differential cross-section are described. Section 3 is devoted to the phenomenological analysis applied to these measurements.

2 Measurement of NC and CC cross sections

Neutral current events, at medium and high Q^2, are basically identified by the presence of an electron (or a positron) in the final state. This is done by the use of the tracking and calorimetry devices covering the range $7^o < \theta_e < 177^o$ and $E'_e > 4$ GeV(at HERA the forward direction $\theta_e = 0^o$ corresponds to the direction of the incoming proton).

The differential cross-section measurement is done by counting the number of events within a kinematic interval in, say x and Q^2. So one of the experimental problem is to achieve a good reconstruction of these kinematic variables from the detector information. With detectors H1 and ZEUS one can use both the outgoing lepton and hadronic informations, namely the polar angles, the momentum and the deposited energy. It is then possible to define the kinematics of each event by using different (and independent) combinations of experimental informations.

In ZEUS the double angle method is used

$$Q^2_{da} = 4E_e^2 \frac{\sin\gamma_h(1+\cos\theta_e)}{\sin\gamma_h + \sin\theta_e - \sin(\gamma_h+\theta_e)}, \quad y_{da} = \frac{\sin\theta_e(1-\cos\gamma_h)}{\sin\gamma_h + \sin\theta_e - \sin(\gamma_h+\theta_e)}$$
$$x_{da} = \frac{E_e}{E_p}\frac{\sin\gamma_h + \sin\theta_e + \sin(\gamma_h+\theta_e)}{\sin\gamma_h + \sin\theta_e - \sin(\gamma_h+\theta_e)}.$$

The hadronic polar angle γ_h is defined by $\tan\gamma_h/2 = \sum_i (E_i - p_{z,i})/P_{t,h}$, where E_i and $p_{z,i}$ are the energy and longitudinal momentum of the final state hadron i and where $P_{t,h}$ is the total transverse momentum of the hadronic final state particles. In H1, the electron method

$$Q^2_e = \frac{(E'_e)^2 \sin^2\theta_e}{1-y_e}, \quad y_e = 1 - \frac{E'_e}{E_e}\sin^2(\theta_e/2)$$

is used to determine Q^2 and x only at high $y > 0.15$ since $dx/x = 1/y\dot{d}E'_e/E'_e$; at low-$y \leq 0.15$ the Σ method is used

$$Q^2_\Sigma = \frac{(E'_e)^2 \sin^2\theta_e}{1 - y_\Sigma}, \;\; y_\Sigma = \frac{\sum_i (E_i - p_{z,i})}{\sum_i (E_i - p_{z,i}) + E'_e(1 - \cos\theta_e)}\,.$$

The reason of the differences between the methods used by H1 and ZEUS are related to the calorimeter performances: H1 possesses finly segmented electromagnetic calorimeters and ZEUS possesses a very good hadronic calorimetry.

The redundancy of the kinematic variable determinations is a crucial point and presents many advantages: minimization of the migration between the 'true' and the measured kinematic variable by choosing one particular method; cross calibration of the various calorimeter devices and studies of photon radiations from the lepton line by comparing leptonic and hadronic informations.

Once the collected events are gathered in the x-Q^2 bins, usual correction factors are applied including: the background subtraction; the efficiency of the event selection; detector acceptance; migration of the kinematics due to detector effects and to the contribution of the higher orders electroweak processes. When possible, these correction factors are determined and/or cross-checked from the data themselves. If not they are determined from a full simulation of the DIS and background processes including the detector response.

For the medium Q^2 we shall describe the preliminary results of the high statistics 1997 data (more than 10000 events per x-Q^2 bins for H1). For high-Q^2 data, the combined 1994-1997 (e^+ beam) data published in ref. [5] are presented.

At medium Q^2 and for the H1 measurements, the main systematic uncertainty sources are: the electron energy scale ($\approx 0.3\%$), the hadronic energy scale ($\approx 2-3\%$), the electron polar angle (≈ 0.3 mrad), photoproduction background at high-y only ($\approx 3\%$ effect on the measurements and), the correction factor (see above) applied to the data (each one is of the order of 1-2%). The overall data normalization (including the luminosity measurement uncertainty) is 1.5 %. The systematics are, in total, of the order of 3% and are larger than statistical uncertainties which are now at the level of 1 % for $Q^2 < 100\text{GeV}^2$.

At high-Q^2 the systematic sources are essentially the same. In ZEUS the statistic and systematic uncertainties amount to 3-5% for the kinematic range $400\text{GeV}^2 < Q^2 < 30000\text{GeV}^2$ considered in the analysis.

In charged current events, the outgoing neutrino escape the detection. Such events are then characterized by a missing transverse energy $p_{t,miss}$ ($p_{t,miss} > 10$ GeV in ZEUS and $p_{t,miss} > 12$ GeV in H1). For the reconstruction of the kinematic variables, one can only use the information of the hadronic final state, i.e. the Jacquet-Blondel method

$$y_{JB} = \frac{\sum_i (E_i - p_{z,i})}{2E_e}, \;\; Q^2_{JB} = \frac{p^2_{t,miss}}{1 - y_{JB}}$$

The statistics is still low, ≈ 900 events for $Q^2 > 400$ GeV^2 in ZEUS. The systematics are dominated by the hadronic energy scale which induces an effect of the order of 10% except at very high Q^2 and very high x where the effect

is above 20%. Other systematic sources related to the $p_{t,miss}$ cut, acceptance correction and photoproduction background subtraction (in the lowest Q^2 bins) lead to measurement uncertainties between 4% and 8%.

3 Phenomenological analysis of inclusive measurements at HERA

As mentioned in the introduction, we shall distinguish the phenomenological analysis of the medium-Q^2 data from the high-Q^2 data. As we are interested in the HERA data, it should be noted that we are considering the region of large $W^2 \gg 10$ GeV^2. Therefore we will not be concerned by the non perturbative effects and the higher-twist effects appearing in this region so that the symbol pQCD appearing below refers to the leading twist of pQCD.

For all details which cannot be given here we refer to ref. [6] and references therein.

3.1 Analysis of medium-Q^2 NC data

In the one boson exchange approximation, the NC differential cross-section reads

$$\frac{d\sigma^{e^\pm p}}{dxdQ^2} = \frac{2\pi\alpha_{em}Y_+}{xQ^4}\sigma_r, \;\; \sigma_r = F_2(x,Q^2) - \frac{y^2}{Y_+}F_L(x,Q^2) \mp \frac{Y_-}{Y_+}xF_3(x,Q^2) \quad (1)$$

where $Y_\pm = 1 \pm (1-y)^2$. The nucleon structure functions are modeled using the quark-parton model and pQCD. In the so called naive parton model one writes

$$F_2(x) = \sum_{i=1}^{n_f} A_i(Q^2)x[q_i(x) + \bar{q}_i(x)]\,,\; F_3(x) = \sum_{i=1}^{n_f} B_i(Q^2)[q_i(x) - \bar{q}_i(x)]$$

where q_i ($\bar{q}_i$)is the density function of the quark (anti-quark) of flavor i, n_f is the number of active flavors and $F_L = 0$. The functions A_i [4] depends on the electric charge e_i ($A_i = e_i^2$ for $Q^2 \ll M_Z^2$) and embodies the effects of the Z exchange and $\gamma - Z$ interference in its Q^2 dependence. Idem for the function B_i [4] except that it vanishes at $Q^2 \ll M_Z^2$.

When QCD is switched on, the higher order contributions in α_s are taken into account. However, in DIS processes mass singularities appear and cannot be regularised without resuming the whole perturbative series. This resumation is done in the restricted kinematic region where $\alpha_s \log Q^2$ is large [6]. This latter region is defined by $Q^2 \gg \Lambda^2 \approx 0.3^2$ GeV^2 and the pCDQ calculations are safe for Q^2 above few GeV^2. In this domain, the parton density functions (pdf) are given by the solution of the DGLAP equations [6]:

$$M_F\frac{\partial q^\pm_{i,NS}}{\partial M_F} = P^\pm_{NS} \otimes q^\pm_{i,NS}$$
$$M_F\frac{\partial}{\partial M_F}\begin{pmatrix}\Sigma(x,Q^2)\\ g(x,Q^2)\end{pmatrix} = \begin{pmatrix}P_{qq} & n_f P_{qg}\\ P_{gq} & P_{gg}\end{pmatrix} \otimes \begin{pmatrix}\Sigma(Q^2)\\ g(Q^2)\end{pmatrix} \quad (2)$$

with $A \otimes B \equiv \int_x^1 A(z)B(x/z)dz/z$ and where $\Sigma = \sum_{i=1}^{n_f} x(q_i + \bar{q}_i)$ is the singlet quark density, $q_{i,NS}^- = q_i^v \equiv q_i - \bar{q}_i$ and $q_{i,NS}^+ = q_i + \bar{q}_i - \Sigma/n_f$ are the two non singlet densities. The splitting functions $P_{i,j} = \alpha_s(M_R^2)P_{i,j}^{(0)} + \alpha_s^2(M_R^2)P_{i,j}^{(1)}$ describes the branching of parton j from parton i, they are computed from pQCD up to the second order. In eq. (2) M_F is the factorization scale (below which the mass singularity is resumed) and M_R is the renormalisation scale (related to the ultra-violet singularity). As the two scales must be chosen somehow arbitrarily, a natural choice for M_F is $\sqrt{Q^2}$, i.e. the virtual mass of the probe. We shall, as usual, also set $M_R = M_F$ for convenience. It is to mention that these equations are universal, i.e. that they are independent of the hard process.

Eq. (2) embodies the mass singularity resumation and therefore it only describes the so called light partons, i.e. the parton of flavour i and mass m_i such $m_i^2/Q^2 \ll 1$. In the medium-Q^2 range one can take the gluon, the up, down and strange quarks as the light partons. For the heavy quarks (charm and bottom) one needs to specify a special scheme. We have chosen the fixed-flavor-scheme (FFS) [7] – suitable in the HERA medium Q^2 range – where the beauty is neglected and where the charm contribution is computed from the boson-gluon-fusion $\gamma g \to c\bar{c}$ plus the α_s^2 corrections. In this scheme the charm is produced 'outside' the hadron. The relation between the pdf and the structure functions depends on the renormalisation scheme. In Next to Leading Log Approximation (NLLA) and in the $\overline{\text{MS}}$ scheme, that we shall use below, one has:

$$F_i(x,Q^2) = x\sum_{i=1}^{n_f}\left[\left(1+\frac{\alpha_s(Q^2)}{2\pi}C_{i,q}\right)\otimes e_i^2(q_i(x,Q^2)+\bar{q}_i(x,Q^2)) + 2\frac{\alpha_s(Q^2)}{2\pi}C_{i,g}\otimes g\right] + F_i^{c\bar{c}}(x,Q^2)$$

for $n_f = 3$ and where $i = 1, 2$ (there is a similar expression for F_3 with $F_3^{c\bar{c}} = 0$); $C_{i,q}$ and $C_{i,g}$ are the coefficient functions depending on the hard process; $F_i^{c\bar{c}}$ is the charm contribution [8], suffices here to say that it depends on m_c^2 and on a renormalisation scale that we choose to be $\sqrt{m_c^2 + Q^2}$. It is to note that $F_L = F_2 - 2xF_1 \neq 0$ in the NNLA.

To solve the system of integro-differential equations (2), one must provide some initial conditions, i.e. some input functions of x at a given Q^2 for each pdf. Since these functions reflect some unknown non-perturbative mechanism, one must parameterize with the help of a set of parameters. As we shall see below, these parameters are determined by comparing the calculations to the experimental data. However, the inclusive DIS data cannot constrain every light flavors: it is clear if one introduce the singlet and a non-singlet $u^+ = xu + x\bar{u} - \Sigma/3$ densities in order to write $\sum_{i=1}^{n_f=3} e_i^2 x[q_i(x,Q^2)+\bar{q}_i(x,Q^2)] = 2/3u^+ + 1/9\Sigma$. There is one important property of the DGLAP kernels $P_{i,j}$: the average total momentum carrying by the partons $\int_0^1(\Sigma + xg)dx$ is independent of Q^2. This quantity is called the momentum sum rule and is usually fixed to 1.

So in principe one may be able to describe the inclusive HERA data by parameterizing the three functions xg, Σ and u^+. But we found that such a description is not adequate for the following reasons:

- it leads systematically to a total momentum carried by the gluons $\int_0^1 xgdx > 60\%$, in contradiction with the results of global fits including specific constrain on xg at high-x [9];
- since the DGLAP equations involve some integrals of the pdf from x to 1, one must also introduce some constraints at higher x, i.e. the fixed target Hydrogen data from NMC and BCDMS [2];
- even if fixed target hydrogen data are included, one is unable to constrain the total momentum carried by the gluons so one must also include the fixed target deuterium data. In this case a second non singlet density must be parameterized (essentially $u + \bar{u} - d - \bar{d}$) but now the valence counting rules $\int_0^1 (u - \bar{u})dx = 2$ and $\int_0^1 (d - \bar{d})dx = 1$ can be applied, under certain assumptions, in order to constrain the momentum sum rule at high-x.

H1 and ZEUS have used the latter option but with different assumptions. We will describe here the fits performed to the 1994 data and to the preliminary 1997 data. Both experiments include their own inclusive measurements and the NMC and BCDMS data.

In H1 two assumptions are made: $\bar{u} = \bar{d}$ and $\bar{s} = s = \bar{d}/2$. The first constraint is in contradiction with the global fit results [9] including the Drell-Yann data but we have found that it does not modify significantly the gluon density at below $x \approx 10^{-2}$. The second assumption comes from the results of the dimuon events of CCFR [10]. Finaly xg, $x\bar{u}$, xu_v and xd_v are parameterized at a given value of Q^2 using the mathematical function $Ax^B(1-x)^C P(x)$ with $P(x) = 1 + Dx + E\sqrt{x}$. The momentum sum-rule and the quark counting rules are applied so that there is 16 free parameters in the H1 fit.

In ZEUS, the two valence quarks are taken from the MRS parameterization [9] and $\bar{s} = s = (\bar{d} + \bar{u})/2$ is also applied. xg, $x(\bar{u} - \bar{d})$ and $x(\bar{u} + \bar{d})$ are parameterized using the above mathematical functions.

Concerning the data-theory comparison, from which the input pdfs have to be determined, both H1 and ZEUS use a χ^2 minimization procedure. The main steps of the fitting procedure are summarized below. For each iteration: 1) the pdf's are parameterized at a given value of Q^2 denoted Q_0^2, it is chosen to be 7 GeV^2 in the ZEUS fit and 4 GeV^2 in the H1 fit, 2) the DGLAP equations are solved numerically in the x-space [11]. 3) the evolved pdf's are convoluted with the coefficient functions to obtain the structure functions. Assuming that all experimental uncertainties are normally distributed a χ^2 is computed. A crucial point of the analysis is the χ^2 expression which permits the use of the correlations introduced by some of the systematic uncertainties:

$$\chi^2 = \sum_{exp} \sum_{dat} \frac{[\mathcal{O}_{exp}^{dat} - \mathcal{O}^{fit} \times (1 - \nu_{exp}\sigma_{exp} - \sum_k \delta_k^{dat}(s_k^{exp}))]^2}{\sigma_{dat,stat}^2 + \sigma_{dat,uncor}^2} + \sum_{exp} \nu_{exp}^2 + \sum_{exp} \sum_k (s_k^{exp})^2$$

where $\mathcal{O}$ stands for the observables (structure functions and differential cross sections). The first two sums run over the data (*dat*) of the various experiments (*exp*); σ_{exp} is the relative overall normalization uncertainty; $\sigma_{dat,stat}$ and $\sigma_{dat,uncor}$ are the statistical error and the uncorrelated systematic error, respectively, corresponding to the datum *dat*; ν_{exp} is the number of standard deviations corresponding to the overall normalization of the experimental sample *exp*; $\delta_k^{dat}(s_k^{exp})$ is the relative shift of the datum *dat* induced by a change by s_k^{exp} standard deviations of the k^{th} correlated systematic uncertainty source of the experiment *exp*. It is estimated by

$$\delta_k^{dat}(s_k^{exp}) = \frac{\mathcal{O}_{exp}^{dat}(s_k^{exp}=+1) - \mathcal{O}_{exp}^{dat}(s_k^{exp}=-1)}{2\mathcal{O}_{exp}^{dat}} s_k^{exp} + \left[\frac{\mathcal{O}_{exp}^{dat}(s_k^{exp}=+1) + \mathcal{O}_{exp}^{dat}(s_k^{exp}=-1)}{2\mathcal{O}_{exp}^{dat}} - 1\right](s_k^{exp})^2$$

where $\mathcal{O}_{exp}^{dat}(s_k^{exp} = \pm 1)$ is the experimental determination of $\mathcal{O}_{exp}^{dat}$ obtained varying by $\pm 1\sigma$ the k^{th} source of uncertainty. Parameters ν_{exp} and s_k^{exp} can be determined if one lets them free during the χ^2 minimization or they can be fixed to zero during the minimization but released during the χ^2 error matrix calculation. In the first case one uses all the experimental informations relying on the correctness of the systematic estimation.

The result of the H1 fit is shown in fig. 1 together with the data. The agreement between data and pQCD is excellent. The gluon density obtained from the ZEUS fit (to the 1994 data) is shown in fig. 2. The xg error bands of this figure include the experimental error propagation as defined in ref. [12] and a theoretical uncertainty including variation of: α_s, the charm mass, the pdf input parameterization form, the value of Q_0^2 and the factorization scale. With the 1997 data one expect a reduction of the experimental uncertainty by a factor two. The model uncertainties will then dominate in the determination of xg, i.e. the third order splitting functions are needed.

3.2 Analysis of high-Q^2 data

The fits applied to the high-Q^2 data differ from the one described in the previous section by a different calculation of the heavy quarks contribution to the structure functions. As $m_c \approx 1.5$ GeV, one has $m_c/Q^2 \ll 1$ at high-Q^2. The large $\alpha_s^n \log^n(Q^2/m_c^2)$ – dominating the calculation of $F_2^{c\bar{c}}$ – must be resumed already at $Q^2 \approx 20$ GeV^2. The massless scheme is therefore used and a rejection data cut of 10 GeV^2 is applied. In this scheme the charm and the beauty are partons and their density functions are obtained by solving the DGLAP equations with the initial conditions $c(x, Q^2 \leq m_c^2) = 0$ and $b(x, Q^2 \leq m_b^2) = 0$. Such fits describe perfectly the HERA NC and CC (see fig. 3 and 5) data above $Q^2 = 10$ GeV^2.

In fig. 3 one can observe the different behavior of e^-p and e^+p cross sections at very high Q^2. This is related to the different sign of the contributions of F_3 to σ_r. Fig. 4 shows $d\sigma/dQ^2$ together with the results of two pQCD fits including

or not the Z exchanges and γZ interferences effects. With the present data, sensitivity to electroweak effects in NC is for the first time observed at HERA.

Up to now we have only described the NC cross-sections and the related structure functions. For CC processes, in the one boson exchange approximation, one has

$$\frac{d\sigma_{CC}^{e^{\pm}p}}{dxdQ^2} = \frac{G_F^2}{2\pi x}\frac{M_W^4}{(M_W^2+Q^2)^2}\Phi_{\pm}(x,Q^2), \tag{3}$$

where G_F is the Fermi constant and where the functions $\Phi_{\pm}$ depends on the CC structure functions (see [4] for example). From eq. (3) one can first remark that the Q^2 slope of the CC differential cross-section (see fig. 6) permits a determination of M_W assuming (or not) the precisely measured value for G_F [13]. To extract M_W, H1 and ZEUS have used two different procedures. In H1, M_W is taken as an extra free parameter (G_F is fixed) of the pQCD fit and in ZEUS, the pdf of CTEQ [9] are used in order to extract M_W and G_F (variations of the pdf choice is taken into account within the errors). The results are

$$\text{H1} : \mathrm{M_W} = 80.9 \pm 3.3(stat.) \pm 1.7(syst.) \pm 3.7(theo)\mathrm{GeV}$$
$$\text{ZEUS} : \mathrm{M_W} = 80.4^{+4.9}_{-2.6}(stat.)^{+2.7}_{-2.0}(syst.)^{+3.3}_{-3.0}(pdf)\mathrm{GeV}$$

and releasing G_F ZEUS obtain

$$M_W = 80.8^{+4.9}_{-4.5}(stat.)^{+5.0}_{-4.3}(syst.)^{+1.4}_{-1.3}(pdf)\mathrm{GeV},$$
$$G_F = [1.171 \pm 0.034(stat.)^{+0.026}_{0.032}(syst.)^{+0.016}_{-0.015}(pdf)] \times 510^{-5}\mathrm{GeV}^{-2}.$$

Let us point out that, concerning the H1 result, the theoretical uncertainty is dominated by the variation of the results when varying the ratio $\bar{d}/\bar{u}$ in the pQCD fit and by the choice of the nuclear corrections applied to the deuterium target data entering the fit. These results, in good agreement with the world average values [13], show that the standard model gives a good description of both space-like (CC in DIS) and time-like (W production in $p\bar{p}$ and e^+e^- collisions) processes.

In order to see the sensitivity of the CC cross section to the pdf, we write $\Phi_{\pm}$ in LO

$$\Phi_+ = x\bar{U} + (1-y)xD; \;\; \Phi_- = xU + (1-y)x\bar{D}$$

with $U = u + c$ and $D = d + s$. From these expressions and from fig. 5 one can remark that: with positron (electron) beams one determine d_v (u_v) at high-x and small-y and $\bar{u} + \bar{c}$ ($\bar{d} + \bar{s}$) at low y. Let us mention that d_v and the sea quarks are basically determined in the global pQCD fits by μd and $\nu(\bar{\nu})F_e$ fixed target data which require some nuclear corrections. Therefore, with the HERA $e^{\pm}p$ CC events one may have, with more statistics, a unique mean to determine properly these quark densities.

In fig 7, $d\sigma/dx$ is shown together with the error band determined by the ZEUS QCD fit (without the CC and NC data described in the present article) and with the results of a recent analysis where an ansatz $d/u \neq 0$ as $x \to 1$ [14] was introduced. Although the statistics is still low one can remark from fig. 7 that this latter hypothesis is not required by the HERA data.

In fig. 8, the preliminary 1998 measurement of $d\sigma^{e^-p}/dx$ is shown. The QCD fit error band is much smaller than in fig. 7 so one expect a better determination of electroweak parameters. The size of the error bands reflect that u_v is much better constrained than d_v in the QCD fits.

3.3 Extraction of F_L

The longitudinal structure function is very hard to determine. It requires to combined data in a given x-Q^2 bin at different beam energies. However, from eq. (1) one observe that at high-y the cross section receives a contribution both from F_2 and F_L. Therefore, assuming F_2 from the result of a pQCD fit (see previous section) applied to the low-$y < 0.35$ data one can determine F_L by subtraction. The result of this operation is shown in fig. 9. To reach lower Q^2, where pQCD is not reliable, another method is used. Writing

$$\frac{\partial \sigma_r}{\partial \log y} = \frac{\partial F_2}{\partial \log y} - 2y^2 \frac{2-y}{Y_+^2} F_L - \frac{y^2}{Y_+} \frac{\partial F_L}{\partial \log y},$$

neglecting $\partial F_L/\partial \log y$ and assuming that $\partial F_2/\partial \log y$ is a linear function of $\log y$, one obtain the results shown in fig. (9). This determination is consistent with the calculation (LO) of pQCD.

4 Conclusion

Recent measurements of medium and high Q^2 differential cross section at HERA have been presented and a determination of F_L was also described. These new DIS inclusive data cover four orders of magnitude Q^2 and five orders of magnitude in x.

In order to test the Quantum Chromo Dynamic, fits based on the DGLAP equation have been performed successfully to the whole data sets, CC and NC, presented in this article. The extraction of the gluon density was described and the result of the analysis of the 1994 data was shown.

At medium Q^2 HERA have reached the limit where the systematic uncertainties dominate the statistical ones. The gluon density which will be determined by the pQCD fit to these data may reach the few percent level of accuracy and a determination of xg and α_s is now foreseen.

Concerning the high Q^2 data, although the statistics of CC events and very high $Q^2 \approx M_Z^2$ NC events is still low, a sensitivity of the results to the Z boson exchanged effects and to M_W was observed. A determination of M_W from $d\sigma^{CC}/dQ^2$ was reported and a good agreement was found with the world average value. Furthermore, comparing $d\sigma^{CC}/dxdQ^2$ with the pQCD calculation

we pointed out that such a measurement offer a unique possibility to pin down – independently of any nuclear effects – d_v and the different components of the proton sea.

Finally, comparing the measurements of $d\sigma^{e^+p}/dxdQ^2$ and $d\sigma^{e^-p}/dQ^2$ we observed, for the first time, the sensitivity of the NC to F_3.

With the high Q^2 NC and CC events a new field of research is touched here. It will be covered precisely by the HERA-2000 upgrade with the help of an increase of luminosity and lepton beam longitudinal polarization.

References

1. H1 Coll., Nucl. Instr. Meth A336, **310** and **348** (1997); The ZEUS detector, status report DESY-1993.
2. BCDMS Coll., Phys. Lett. B223**3**, 485 (1989); Phys. Lett. B237, **592** (1989); NMC Coll. Nucl. Phys. B483, **3** (1997).
3. H1 Coll. Nucl. Phys. B470, **3** (1996); ZEUS Coll. Eur. Phys. J. C7, **609** (1999), see also M. Botje, DESY 99-038 for the ZEUS pQCD fits.
4. See for a recent review: A.M. Cooper-Sarkar, R.C. Devenish and A. De Roeck, Int. J. Mod. Phys. A13, **3385** (1998).
5. H1 Coll., DESY 99-107; ZEUS Coll., DESY 99-56 and DESY 99-59.
6. W. Furmanski and R. Petronzio, Z. Phys. C1, **293** (1982).
7. M. Gluck, E. Reya and M. Stratmann, Nucl. Phys. B422, **37** (1994).
8. E. Laenen et al., Nucl. Phys. B392, **162** and 229 (1993); Phys. Lett. B291, **325** (1992).
9. CTEQ4 Coll., Phys. Rev. D55, **1280** (1997); MRS Coll., Phys. Rev. D51, **4756** (1995).
10. CCFR Coll., Z. Phys. C65, **189** (1995).
11. C. Pascaud and F. Zomer, DESY 96-266; J. Blümlein et al., in Proc. of the Workshop on Future Physics at HERA, G. Ingelman, A. De Roeck and R. Klanner eds., **23** DESY (1996).
12. C. Pascaud and F. Zomer, LAL 95-05.
13. Particle Data Group, Eur. J. C3, **1** (1998).
14. U.K. Yand and A. Bodek, Phys. Rev. Lett. 82, **2467** (1999).
15. See for instance Proc. of the Workshop on Future Physics at HERA, G. Ingelman, A. De Roeck and R. Klanner eds. DESY (1996).

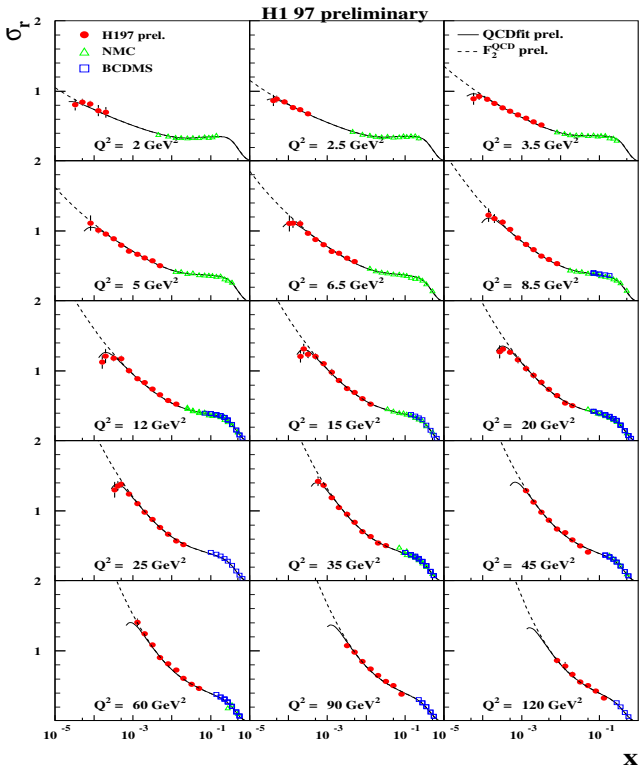

Fig. 1. H1 preliminary measurements of σ^r together with the result of a pQCD fit (see text).

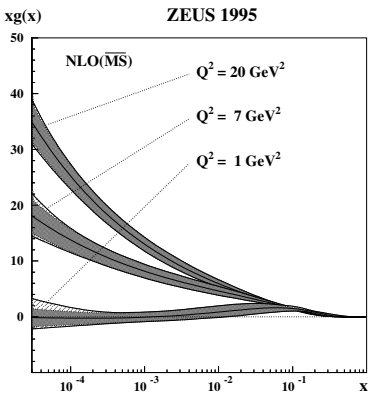

12

Fig. 2. xg extracted from the ZEUS fit to the 1994 data for three values of Q^2. Error bands contain the experimental error propagation and a theoretical error estimation (see text).

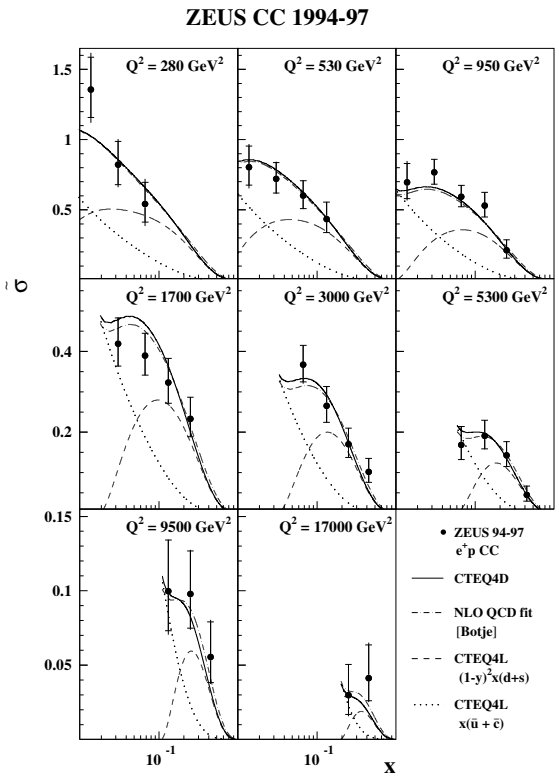

Fig. 3. High Q^2 H1 measurements of σ_r (eq. 1) compared with pQCD fit results (see text).

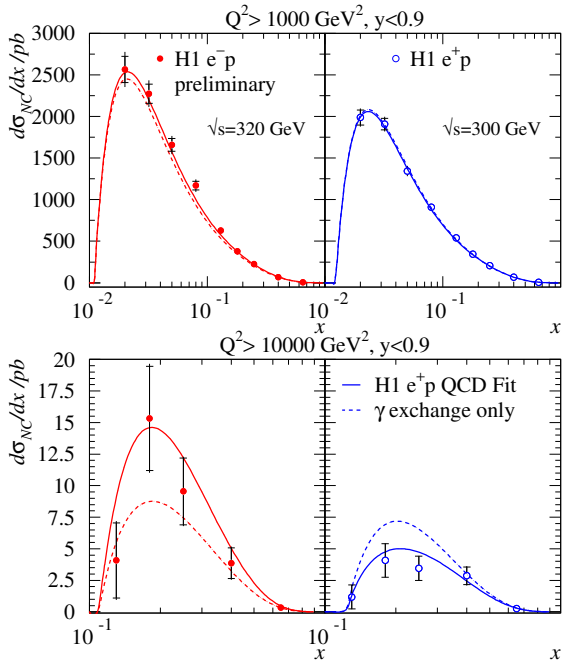

Fig. 4. H1 measurements of $d\sigma/dQ^2$ together with various pQCD results (see text).

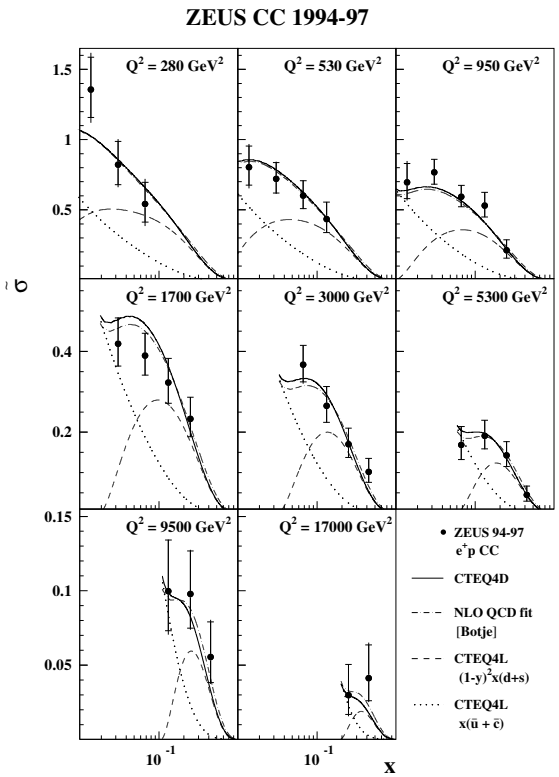

Fig. 5. ZEUS measurements of Φ_+ together with various pQCD calculations (see text).

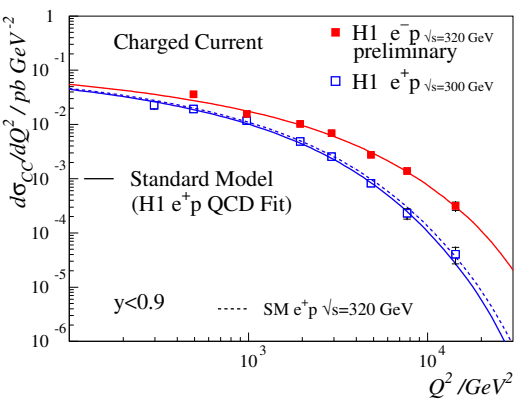

Fig. 6. H1 measurements of $d\sigma^{CC}/dQ^2$ together with the pQCD fit results.

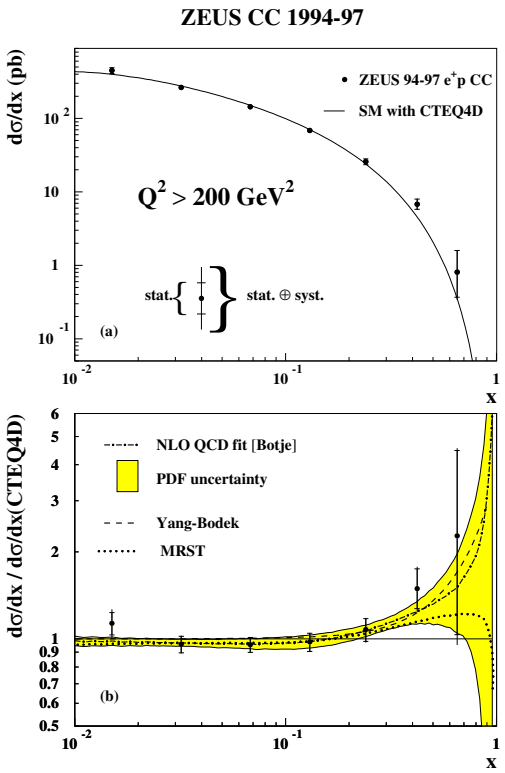

Fig. 7. ZEUS measurements of $d\sigma^{CC}/dx$ together with various pQCD results (see text).

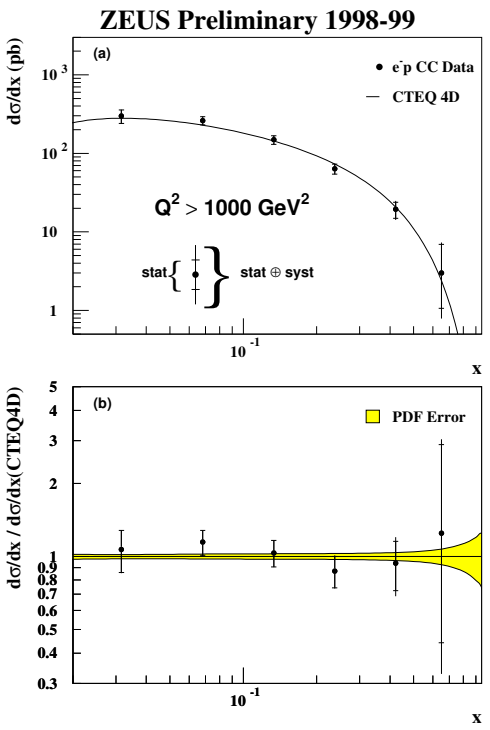

Fig. 8. ZEUS measurements of $d\sigma^{CC}/dx$ together with the pQCD fit result.

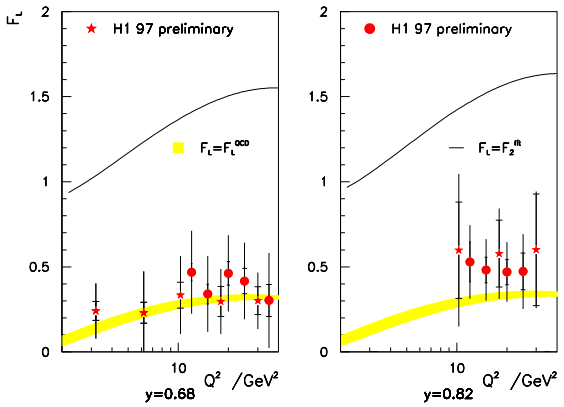

Fig. 9. H1 determination of F_L. The full points correspond to the subtraction method and the stars to the derivative method (see text).